Desalination and Water Treatment
www.deswater.com

doi: 10.5004/dwt.2021.27114

224 (2021) 168–177
June

Magnetic nanoadsorbents derived from magnetite and graphene oxide for simultaneous adsorption of nickel ion, methylparaben, and reactive black 5

Hua-Wei Chen[a,*], Chyow-San Chiou[b], Yo-Ping Wu[a], Chun-Hao Chang[b], Yi-Hung Lai[a]

[a]*Department of Chemical and Materials Engineering, National Ilan University, 1, Sec. 1, Shen-Lung Road, Yi-Lan 260, Taiwan, Tel. 886-3-9317498; Fax: 886-3-9357025; email: hwchen@niu.edu.tw (H.-W. Chen)*
[b]*Department of Environmental Engineering, National Ilan University, 1, Sec. 1, Shen-Lung Road, Yi-Lan 260, Taiwan*

Received 11 August 2020; Accepted 4 February 2021

ABSTRACT

The purpose of this study was to investigate magnetic nanoadsorbents (GO/Fe_3O_4) derived from magnetite (Fe_3O_4) and graphene oxide (GO) for simultaneous removal of nickel ion (Ni(II)), methylparaben (MP), and reactive black 5 (RB5). As a result, the maximum adsorption capacity in aqueous solution for Ni(II), MP, and RB5 was 15.5, 20.69, and 63.18 mg g^{-1} in single-component system, respectively. The adsorption of Ni(II), MP, and RB5 onto GO/Fe_3O_4 reveals good agreement with the Langmuir adsorption isotherms and pseudo-second-order model. The adsorption capacity suppressed for MP with increasing RB5 concentration in MP–RB5 binary system. However, the adsorption capacity for Ni(II) almost was not affected with increasing MP and RB5 concentration in binary system. The mechanisms of GO/Fe_3O_4 for the adsorption of Ni(II), MP, and RB5 are probably dominated by π–π interaction, electrostatic attraction, both π–π interaction and electrostatic attraction, respectively. The optimum ethanol concentration to desorb methylparaben from GO/Fe_3O_4 is 95% with a three times adsorption–desorption cycle by the recovery of magnetic force due to the detachment of the shell (graphene). Conclusively, GO/Fe_3O_4 has good adsorption performance and is easily reused; these are important factors contributing to its potential practical application.

Keywords: Adsorption; Graphene oxide; Magnetic nanoadsorbents; Methylparaben; Nickel ion; Reactive black 5

1. Introduction

Heavy metals, organics, and dyes generally coexist in the deleterious wastewater generated from domestic, agricultural, and industrial sources [1–4]. Treatment processes for anionic dye, organic contaminated waste streams, and heavy cations include advanced oxidation [3], electrocoagulation [1,5,6], chemical precipitation [6], filtration [7], electrodeposition [8], ion exchange [9], and adsorption [2,4,9,10], etc. Each of these methods has some disadvantages in their application. However, the adsorption is considered as an effective and cost-efficient method, and provides an economical approach capable of removing various pollutants from aqueous solutions [4,11–13] if the adsorbents used within the setup could be recovered and regenerated by an appropriate separation and desorption process.

Graphene oxide (GO) has been applied to adsorb heavy metals, organic compounds and anionic dyes in environmental contamination [14–16], but it is related to the difficult recovery from aqueous phase. Different methods for synthesis of GO from graphite, one of the most known is the improved Hummers method in which potassium permanganate is used as an oxidizing agent in a mixture of sulfuric acid: phosphoric acid in a volume ratio of 9:1 [14,15]. The synthesis of date syrup-based graphene sand hybrid (D-GSH) was performed using the research proposed by Khan et al. [16], the graphitization of date

* Corresponding author.

syrup and desert sand was mixed in a 5:2 weight ratio for 1 h by overnight drying at 80°C. The nanosized magnetic materials have a great potential to solve this problem due to their extremely small size, high surface area, cost-effectiveness, high removal efficiency, the absence of internal diffusion resistance, and unique advantage of easy recovery under external magnetic field [3,17,18]. Moreover, the magnetic separation is beneficial to the environment without the extra production of contaminants and energy consumption [17,19].

Parabens are widely used as preservatives in personal care products (PCPs) such as medicines, foods and cosmetics [20]. In cosmetics alone, parabens (such as methylparaben, ethylparaben, propylparaben, etc.) are found in more than 22,000 products, with a maximum content of 0.4% for each paraben species and 0.8% in combination [21]. Parabens can destroy the cell membranes of microbes, leading to intracellular protein denaturation and inhibit the enzyme activity of microbial cells [20]. However, several researchers have proposed that parabens have a potential effect similar to that of estrogen, and that extensive use of parabens can be harmful to human health [22,23]. Methylparaben is the most widely used preservative employed in cosmetic products owing to its broad antimicrobial spectrum, effectiveness and low production cost [20,22]. It was determined that most PCPs found in influent waters, had the preservatives methylparaben and propylparaben used in the highest concentrations with values of 5,613 and 1,945 ng/L, respectively [22,24]. In addition, exposure to highly nickel-polluted environments potentially resulted in various pathological effects in humans, such as contact allergens, contact dermatitis, cancer, and lung diseases [25,26]. The presence of nickel in cosmetics is forbidden by European Law 76/768/EEC, and cosmetics should not contain more than 5 ppm of nickel in order to minimize the risk of sensitization due to the high absorption via the peri-ocular areas and lips every day [27]. Reactive black 5 (RB5) is currently used in textile industries for dyeing materials such as cellulose and fibers [28]. The discharge of RB5 to the environment posed major threat to public health such as acute bronchitis, skin irritations, and mutations [28,29].

Graphene oxide (GO) has the performance in the application to adsorb heavy metals, organic compounds and anionic dyes in environmental contamination, but it is related to the difficulty for the recovery from aqueous phase. The objective of this study was to synthesize magnetic nanoadsorbents (GO/Fe_3O_4) derived from magnetite and graphene oxide for the removal of Ni(II), MP, and RB5. The removal performances of GO/Fe_3O_4 were examined in detail using both kinetics and equilibrium adsorption isotherm analyses. Multi-component adsorption behaviors were also investigated using binary systems including Ni(II)–MP, Ni(II)–RB5 and MP–RB5.

2. Materials and methods

2.1. Synthesis of adsorbents

For the purpose of this study, all the chemicals purchased from various suppliers, were of a reagent grade. The details of the experiments conducted are given in Supporting Information (SI). In brief, graphene oxide (GO) was synthesized by using the modified Hummers method [15] through oxidation of graphite powder. The previously synthesized GO gel (100 mL) was suspended in 500 mL of D.I. water by sonication following which the mole ratio (2:1) between $FeCl_3$ and $FeSO_4$ was added to prepare the slurry solution with a nitrogen purge gas. The GO/Fe_3O_4 composite was synthesized using an ammonia solution and hydrazine hydrate for 1 h at a temperature of 90°C and a pH of 10. After ethanol and D.I. water washing several times, GO/Fe_3O_4 was separated by the external magnetic force and then vacuum dried.

2.2. Adsorption and desorption experiments

The effects of the adsorption isotherm and kinetics on the adsorption of methylparaben from aqueous solutions for the magnetic adsorbents (GO/Fe_3O_4) were studied in batch experiments. The loading of magnetic adsorbents was 10 g L^{-1} after the adsorption reached equilibrium. The magnetic adsorbents were collected via an external magnetic force after the equilibrium time of 24 h.

The determination of desorption efficiency was carried out with 0–100% ethanol. The 10 g L^{-1} loading of magnetic adsorbents adsorbed with methylparaben was added into ethanol under thermostatic shaking for 24 h. The concentration of MP and RB5 was determined by standard spectrophotometric methods using a UV/VIS spectrophotometer (UV-1800, Shimadzu, Japan). The measurement of nickel was carried out with an atomic absorption spectrometer (Z-2300, Hitachi, Japan) at a wavelength of 236.0 nm. The magnetic behavior, the specific surface area, and the functional groups of the synthesized adsorbents were measured by a vibrating sample magnetometer (VSM, Lake Shore 7407, Lake Shore, USA), FTIR spectrometer (Spectrum 100, PerkinElmer, USA), and particle size analyzer (ASAP 2000C, Micromeritics, USA), respectively.

3. Results and discussion

3.1. Characterization of magnetic nanoadsorbents

According to the Brunauer–Emmett–Teller (BET) surface area measurements, the specific surface area of Fe_3O_4, GO, and GO/Fe_3O_4 is listed in Table 1. When Fe_3O_4 was modified with the graphene oxide (GO), the BET surface area (GO/Fe_3O_4) increased to 143.53 $m^2 g^{-1}$, and it was also nearly equal to the surface area of GO.

In order to investigate the morphology of obtained materials, Fig. 1 shows TEM images of GO/Fe_3O_4. The morphology of the synthesized GO/Fe_3O_4 was roughly

Table 1
Brunauer–Emmett–Teller surface area of Fe_3O_4 and GO/Fe_3O_4

Magnetic catalyst	Surface area ($m^2 g^{-1}$)
Fe_3O_4	18.06
Graphite	8.49
Graphene oxide (GO)	130.47
GO/Fe_3O_4	143.53

spherical nanostructures with the size from 20 to 40 nm, and both the outline of graphene oxide and magnetite nanoparticles can be clearly observed. The results revealed that many Fe_3O_4 nanoparticle aggregates uniformly dispersed on the 2D surface of graphene oxide nanosheets. There are also many wrinkles on GO/Fe_3O_4 surface possibly owing to the rolling up and surrounding effect of graphene oxide planes. The similar results revealed that the macroporous walls of porous reduced graphene oxide/single-walled carbon nanotubes also consisted of wrinkled and flexible graphene sheets [30].

The magnetic properties of GO/Fe_3O_4 were measured by VSM as shown in Fig. 2. The mass saturation magnetization (Ms) of Fe_3O_4 was 57.31 emu g^{-1}, which is in good agreement with the value in a previous study [18,31]. A decrease in Ms from 57.31 to 30.26 emu g^{-1} was observed in the case of GO/Fe_3O_4 owing to the contribution of the nonmagnetic GO shell to the overall particles mass. Related results [13] also showed that the saturation magnetization of magnetite particles was decreased after the coating of gold shell. This magnetic measurements in this study also revealed that the magnetic adsorbents exhibited a paramagnetic behavior at room temperature, and similar results also were presented in other studies [9,13].

The FT-IR spectra of Fe_3O_4 and the magnetic nanoparticle synthesized with graphene oxide (GO/Fe_3O_4) are presented in Fig. 3. The absorption bands of GO/Fe_3O_4 in this study appeared at 3,411; 1,624; 1,383; 1,055; and 577 cm^{-1} attributed to the skeletal vibration of CO–H, C=C, C=O, C-O, and Fe–O bonds, respectively and in good agreement with previous reports [32,33]. The presence of a strong peak at 577 cm^{-1} for Fe–O vibration confirmed that a large number of Fe_3O_4 particles were successfully loaded on the GO surface. The appearance of a signal at 577 cm^{-1}, which is attributed to Fe_3O_4 and more importantly, the absence of peaks at 1,733 and 3,411 cm^{-1}, assigned to stretching of the C=O and CO–H of carboxyl groups, respectively. Thus, the comparison of characteristic peaks between GO/Fe_3O_4 and Fe_3O_4 indicated that Fe_3O_4 particles were successfully attached onto the GO surface.

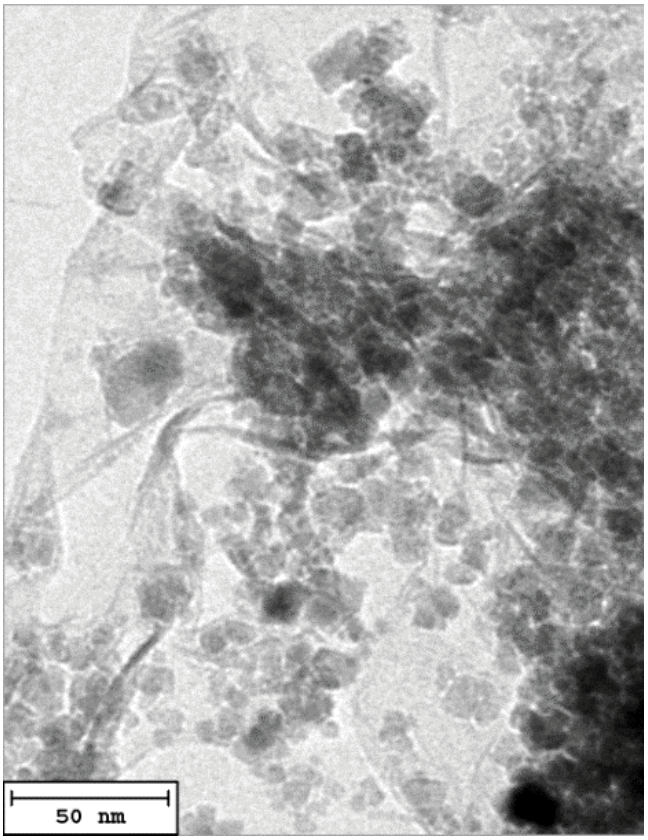

Fig. 1. TEM image of magnetic nanoadsorbents (GO/Fe_3O_4).

3.2. Adsorption isotherms and behaviors of GO/Fe_3O_4

The pH level in the solution is one of the most important factors affecting the adsorption of metal ions. Nickel species including Ni^{2+}, $Ni(OH)^+$, $Ni(OH)_2$, $Ni(OH)_3^-$ and $Ni(OH)_4^2$ are presented both in the acidic and basic regions depending on the pH of the solution [34]. In single-component system, the adsorptions of Ni(II), MP, and RB5

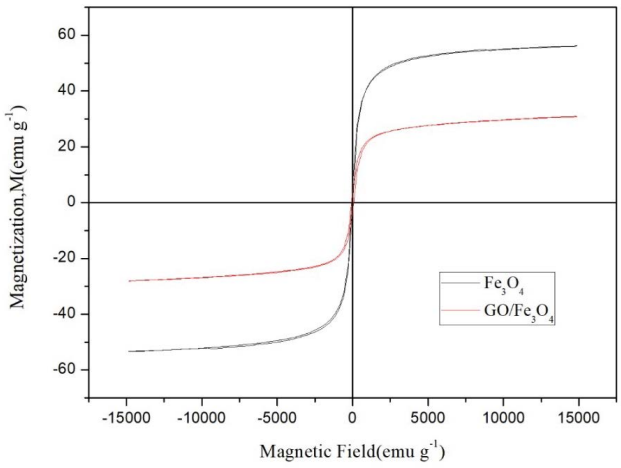

Fig. 2. Magnetization vs. applied magnetic field for Fe_3O_4 and GO/Fe_3O_4.

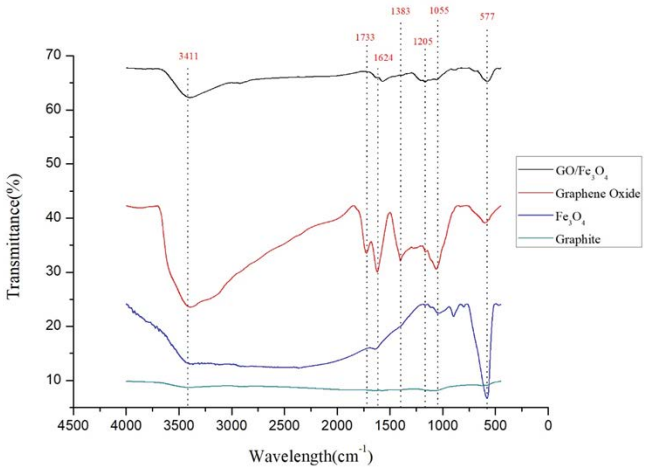

Fig. 3. FT-IR spectra of Fe_3O_4 and GO/Fe_3O_4.

by GO/Fe_3O_4 with different pH levels at 10 g L^{-1} loading, 24 h reaction time, and 298 K is presented in Fig. 4. The results reveal that the adsorption behavior of MP was almost pH-independent because the strong adsorptive interactions of MP onto GO/Fe_3O_4 resulted from π–π electron donor–acceptor interactions between the phenyl molecules and graphene nanosheets of GO/Fe_3O_4. The research carried out by Xiao et al. [35] also reported that the π–π stacking adsorption mechanism confirmed reduced graphene oxide to be used as a broad-spectrum adsorbent with high efficiency for dye contaminants.

The adsorption efficiencies decreased from 99.1% to 70.4% as pH level increased from 2 to 7 within 120 min contact time at 25°C, initial RB5 concentration of 600 ppm, and adsorbents loading of 10 g L^{-1}. The higher adsorption efficiencies of RB5 at lower pH (from pH 2 to pH 6) could be ascribed to π–π interactions and electrostatic attraction between the negatively charged molecules and the positively charged GO/Fe_3O_4 surfaces, which were replaced by repulsive electrostatic forces as pH level was increased. The adsorption efficiencies approximately were kept constant at 70% from pH 7 to 10 only due to π–π interactions. A similar trend has been previously proposed by the research [36].

The adsorption efficiency of Ni(II) by GO/Fe_3O_4 at pH 2.0 was 35.3% and remained at 99.7% above to pH 9.0. The removals of Ni(II) by GO/Fe_3O_4 were increased with an increase of pH value from 2.0 to 7.0, where Ni^{2+} cation is the dominant species for nickel. The carboxyl groups on graphene nanosheets of GO/Fe_3O_4 would lead to electrostatic attraction of Ni^{2+} to be adsorbed at low solution pH level. Furthermore, a relatively high concentration of protons would strongly compete with Ni^{2+} for the surface sites of GO/Fe_3O_4 in solutions with low pH values, so that the adsorption of Ni^{2+} was significantly decreased. However, nickel ion was removed by both adsorption and precipitation when the solution pH value exceeded 8.0 owing to the precipitation of nickel(II) hydroxide. Thus, all further experiments for adsorption of Ni^{2+} in this study were controlled at pH of 6.0.

In order to further understand the adsorption mechanism of Ni(II) ions onto magnetic nanoadsorbents, the point of zero charge (PZC) of GO/Fe_3O_4 at a certain pH was measured and is shown in Fig. 5. The results revealed that PZC of Fe_3O_4 and PS/Fe_3O_4 were 6.6 and 8.2, respectively. The trend of the PZC analysis is in accord with the increase in adsorption capacities as the increase of pH level from 2 to 7. The effect of pH on adsorption and on PZC analysis of the adsorbents showed that the driving force of the Ni(II) ions adsorption on GO/Fe_3O_4 is electrostatic attraction between the carboxyl groups surface and positively charged Ni(II) ions. As a result of adsorption and PZC analysis, it became difficult for Ni^{2+} to come into close contact with the surface of GO/Fe_3O_4 and be adsorbed onto it; this resulted in poor adsorption performance for Ni^{2+} in a solution with pH ≤ 5.

The data equilibrium isotherms of methylparaben and nickel ion adsorptions by GO/Fe_3O_4 at 10 g L^{-1} adsorbent loading, 298 K and 24 h reaction time were listed in Table 2, and these are fitted by the Langmuir and Freundlich isotherm equations [2,20]. The Langmuir equation can be expressed as:

$$\frac{C_e}{q_e} = \frac{C_e}{q_m} + \frac{1}{q_m K_L} \tag{1}$$

where q_e and q_m are the equilibrium and maximum adsorption capacities of methylparaben on the adsorbents in mg g^{-1}; C_e is the final concentration at equilibrium in mg L^{-1}; and K_L is the Langmuir adsorption constant in L mg^{-1}. The linear form of the Freundlich equation can be represented as follows:

$$\log q_e = \log k_F + \frac{1}{n}\log C_e \tag{2}$$

where K_F and n are the Freundlich constants representing the adsorption capacity and intensity, respectively.

The values of q_m and K_L, as determined from the slope and intercept of the linear plots of C_e/q_e vs. C_e, and the values of K_F and $1/n$, as determined from the slope and intercept of the linear plot of $\log q_e$ vs. $\log C_e$, are also listed in Table 2.

The resulting correlation coefficient of GO/Fe_3O_4 for the adsorption of Ni(II), MP, and RB5 indicated that the

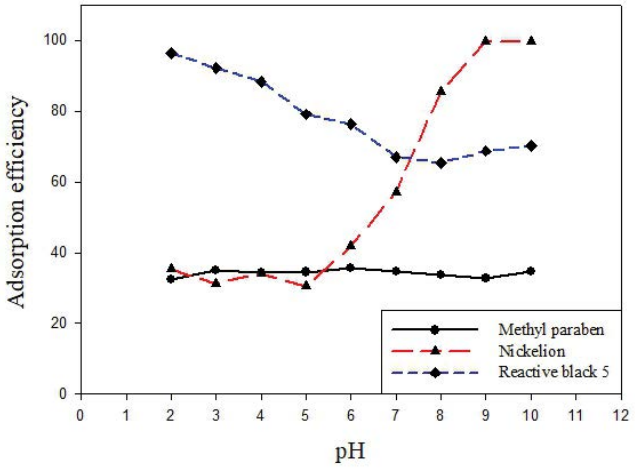

Fig. 4. Effect of pH on the adsorption of Ni(II), MP, and RB5.

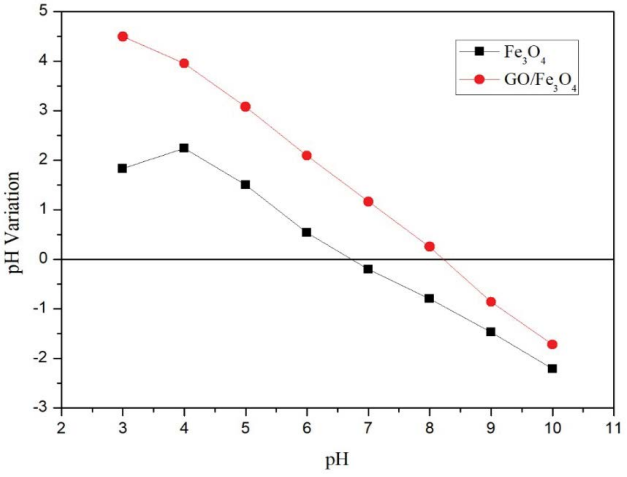

Fig. 5. Effect of pH values on zeta potential of GO/Fe_3O_4.

Table 2
Values of parameters of the different types of adsorption isotherm models fitting to the experimental results of different initial concentration at 25°C on the GO/Fe_3O_4

Treatments	Langmuir			Freundlich		
	q_m (mg/g)	K_L (L/mg)	R^2	n	K_F	R^2
Ni(II)	15.53	0.0211	0.9873	2.99	1.98	0.9673
MP	20.69	0.0113	0.9662	2.70	1.96	0.9404
RB5	63.18	0.0710	0.9937	8.57	37.85	0.9357

data fit well with Langmuir equations. The Langmuir isotherm indicated the maximum adsorption capacity (q_m) of Ni(II), MP, and RB5 was 15.53, 20.69, and 63.18 mg g^{-1}, respectively. In similar experimental conditions, q_m of GO/Fe_3O_4 for the MP adsorption at 298 K was 34 times greater than that of the magnetite with the polystyrene coating (0.60 mg g^{-1}) in the previous study [20]. This is possible due to the contribution of the higher surface area of GO/Fe_3O_4 in agreement with the results of BET measurement.

3.3. Kinetics and thermodynamics of adsorption

The pseudo-first-order and pseudo-second-order kinetic models were applied to model the adsorption kinetics onto GO/Fe_3O_4 in order to explore the adsorption mechanism of adsorption. The Lagergren and Svenska rate equation, which is the first rate equation developed for adsorption in liquid/solid systems, is based on the solid capacity. The pseudo-first-order model [37,38] for adsorption in liquid/solid systems can be expressed as follows:

$$\log\left(q_e - q_t\right) = \log q_e - \frac{k_1}{2.303}t \tag{3}$$

where q_e and q_t are the amounts of methylparaben adsorbed (mg g^{-1}) at equilibrium and at time t, respectively; and k_1 is the kinetic rate constant for the pseudo-first-order (min^{-1}), which can be obtained from the plots of $\ln(q_e - q_t)$ against t at various temperatures of operation, as shown in Table 3.

Based on the solid capacity, the pseudo-second-order equation [33,38] can be expressed linearly as follows:

$$\frac{t}{q_t} = \frac{1}{k_2 q_e^2} + \frac{1}{q_e}t \tag{4}$$

A linear plot of t/q_t against t, as shown in Table 3, gives a slope of $1/q_e$ and an intercept $1/k_2q_e^2$, whereby k_2, the kinetic rate constant for the pseudo-second-order model (g mg^{-1} min^{-1}), can be determined.

According to the linearity of the plots, the two models reveal their applicability in describing the adsorption process of Ni(II), MP, and RB5. The results suggested that the adsorption processes of GO/Fe_3O_4 for Ni(II), MP, and RB5 follow the second-order kinetic model, indicating that the adsorption process was quite rapid. Similar results [20,31] proposed that the kinetics of MP and RB5 adsorptions also showed that the reactions are pseudo-second order, and the adsorption isotherm well followed the Langmuir model [20,31]. Furthermore, the research by Lin et al. [39] also revealed that the adsorption kinetics of nickel ions was established and was well agreed with the second-order model and Langmuir isotherm for biosorbents using succinylation hay with 5 g L^{-1} of biochar composites.

The temperature dependence of the kinetic parameter k_2 in Table 3 can be described by the Arrhenius equation (Eq. (7)):

$$\ln k = \ln A - \frac{E_a}{RT} \tag{5}$$

where A, E_a, T, and R are the frequency factors, activation energy, temperature (K) and gas constant, respectively. The activation energy is calculated by the coefficient of k_2 in pseudo-second-order kinetic model. By plotting $\ln k_2$ against $1/T$ (1/K), the reaction temperatures for Ni(II), MP, and RB5 were given E_a values of 13.06, 11.02, and 10.34 kJ mol^{-1}, respectively.

The magnitude of the activation energy is able to explain the mechanism occurring for the binding, whether the binding is through physisorption or through chemisorption. As the activation energy is less than 40 kJ mol^{-1}, the mechanism occurring is a physical attraction (physisorption) with the quick rate of the reaction [40,41]. Chemisorption generally has activation energies above 40 kJ/mol because the chemical process requires more energy [40]. Whereas, the rate of the reaction is rather slow as the activation energy is greater than 120 kJ mol^{-1} [41]. In summary, the results from activation energy proposed that the adsorption process for Ni(II), MP, and RB5 to GO/Fe_3O_4 occurs rapidly through physisorption due to the activation energies below 40 kJ/mol, and the conclusion is in accordance with that of Langmuir isotherm.

3.4. Effect of initial pollutant concentration in multi-component system

The effects of Ni(II), MP, and RB5 on adsorption performance of Fe_3O_4/GO in binary system were evaluated using the ratio of adsorption capacity (R) as follows:

$$R = \frac{q_{b,i}}{q_{s,i}} \tag{6}$$

where $q_{b,i}$ is the adsorption capacity for component i in the binary system (mg g^{-1}) and $q_{s,i}$ is the adsorption capacity for

component *i* with the same initial concentration in a single-component system. It was proposed that [42]: if $R < 1$, the adsorption of component *i* was inhibited by co-component. If $R = 1$, the adsorption of component *i* was not affected by the presence of the co-component.

As depicted in Fig. 6, the effects of the initial pollutant concentrations on *R* value and the adsorption of Ni(II), MP, and RB5 onto Fe_3O_4/GO were investigated in single system and binary system. The results from Fig. 6a obtained that adsorption capacity of MP at the initial MP concentration of 200 mg L^{-1} onto Fe_3O_4/GO significantly decreased as the increase of RB5 from 100 to 600 mg L^{-1}. At the initial MP concentration of 200 mg L^{-1}, the adsorption capacity for MP was 10.25 mg g^{-1} in single-component system and 7.21 m g^{-1} at the initial MP concentration of 600 mg L^{-1} in MP–RB5 binary system. The adsorption capacity of MP in MP–RB5 binary solutions was only 28.19% of that in single-component system. The evaluated results that *R* value was less than 1 for adsorption of MP onto Fe_3O_4/GO in MP–RB5 binary system (Fig. 6b), which be attributed to the competitive adsorption between MP and RB5 at the same sites. The adsorption of RB5 onto GO/Fe3O4 was better than that of MP in MP–RB5 binary system. The dominant mechanisms of the adsorption of anionic dye RB5 were π–π interaction between RB5 and GO/Fe_3O_4 and electrostatic force, but that of MP (non-ionic molecule) was only π–π interaction between MP and GO/Fe_3O_4.

At the initial Ni(II) concentration of 200 mg L^{-1}, the adsorption capacity of Ni(II) almost was not affected with increasing MP concentration from 100 to 600 ppm in Ni(II)–MP binary system (Fig. 6c). However, *R* value was almost equal to 1 for MP adsorption in Ni(II)–MP binary system (Fig. 6d), thus discarding the competitive adsorption between Ni(II) and MP. The adsorption capacity of Ni(II) at the initial Ni(II) concentration of 200 mg L^{-1} was independent on the concentration of RB5 in Ni(II)–RB5 binary system (Fig. 6e). Similar study also reported that the sorption capacity for Cd(II) almost was not affected for methyl blue with increasing Cd(II) concentration [42]. Furthermore, RB5 had no effect on the adsorption of Ni(II) onto Fe_3O_4/GO in Ni(II)–RB5 binary solutions (Fig. 6f), leading to R value approximately equal to 1. Possibly due to different adsorption sites, the adsorption capacity of Ni(II) was independent on the RB5 concentration and MP concentration in Ni(II)–RB5 and Ni(II)–MP binary system, respectively. In addition, the study also proposed that heavy metal cations (Cu(II), Zn(II), Cd(II), and Fe(II)) adsorption and phenol adsorption do not proceed with the same mechanism [43].

Noticeably, Ni(II) could occupy different adsorption sites on the Fe_3O_4/GO adsorbent with RB5 and MP. Furthermore, MP adsorption was greatly suppressed by the presence of RB5 because MP and RB5 would occupy for limited adsorption sites. From the above analysis and discussion, the mechanisms presumably involved in the adsorption of MP, RB5, and Ni(II) on Fe_3O_4/GO, with a special focus on

Table 4
Desorption efficiency of Ni(II), MP, and RB5 in solutions with different concentrations of HNO_3, ethanol, and NaOH solutions at 24 h reaction time, 10 g L^{-1} loading, and 298 K

Treatments	Solutions	Concentration	Desorption efficiency (%)
Ni(II)	HNO_3	0.005 M	55.4
		0.05 M	56.1
		0.1 M	56.2
		0.5 M	56.8
		1.0 M	57.2
		2.0 M	57.4
MP	Ethanol	40%	64.7
		50%	75.2
		60%	80.3
		70%	81.7
		80%	91.5
		95%	98.7
RB5	NaOH	0.005 M	25.0
		0.01 M	28.8
		0.1 M	32.6
		0.5 M	30.8
		1.0 M	30.2
		2.0 M	29.7

Table 3
Parameter values of the kinetics models fitting to the experimental results for Ni(II), MP, and RB5 adsorptions on GO/Fe_3O_4 at 10 g L^{-1} loading, and 50 mg L^{-1} initial concentration

Treatments		R^2		Rate constants	Activated energy
T (°C)		1st order	2nd order	k_2 (g mg^{-1} min^{-1})	E_a (kJ mol^{-1})
Ni(II)	10	0.8815	0.9838	0.0051	13.06
	25	0.9636	0.9863	0.0062	
	40	0.6326	0.9938	0.0087	
MP	15	0.9214	0.9985	0.0469	11.02
	37	0.9640	0.9992	0.0533	
	55	0.8831	0.9990	0.0842	
RB5	10	0.8618	0.9630	0.0005	10.34
	25	0.8194	0.9580	0.0005	
	40	0.7820	0.9768	0.0008	

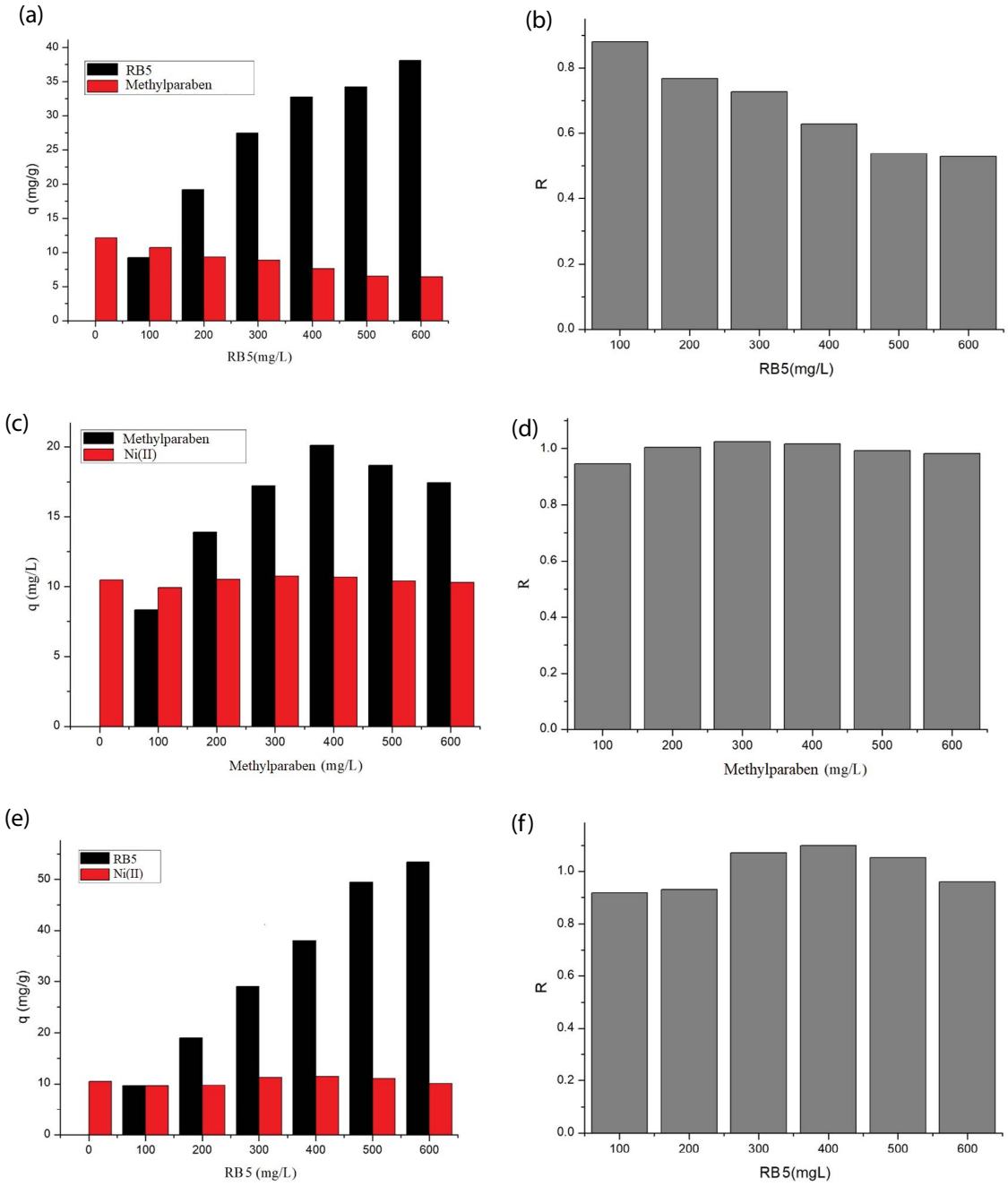

Fig. 6. Effect of initial pollutant concentration on the adsorption and ratio of adsorption capacities (*R*) in binary system including (a) MP–RB5, (b) *R*: MP–RB5, (c) Ni(II)–MP, (d) *R*: Ni(II)–MP, (e) Ni(II)–RB5, and (f) *R*: Ni(II)–RB5.

the roles of π–π interaction and electrostatic attraction as schematically illustrated in Fig. 7.

3.5. Desorption and repeated use

As depicted in Table 4, HNO_3, ethanol, and NaOH solutions with different concentrations at 298 K, 24 h contact time, and 10 g L^{-1} loading were evaluated in desorption experiments for Ni(II), MP, and RB5, respectively. The amounts of MP desorption on GO/Fe_3O_4 greatly increased along with the increases in ethanol concentration. The adsorbed MP on GO/Fe_3O_4 was almost desorbed when the ethanol concentration was 95%. These results indicated the existence of a weak interaction between the MP and GO/Fe_3O_4 and that the adsorption process was almost completely reversible. In addition, the results obtained that Ni(II) desorption efficiencies were kept constant at different HNO_3 concentrations. Furthermore, the results of the RB5 desorption was interesting to note since maximum desorption efficiency was achieved at an NaOH concentration greater than 0.1 M and

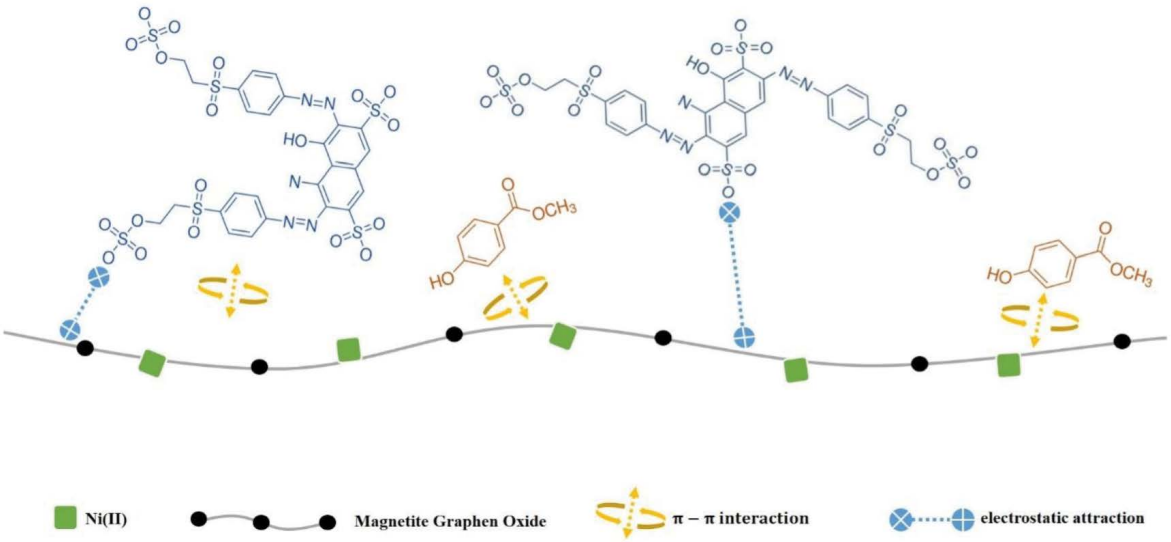

Fig. 7. Ratio of adsorption capacities.

Table 5
Reuse performance of GO/Fe_3O_4 adsorbents at 298 K, 50 mg L^{-1} initial concentrations, and 10 g L^{-1} loading

Cycle (time)	GO/Fe_3O_4 adsorption (mg g^{-1})
1	17.5
2	16.9
3	14.3

desorption efficiencies were kept constant at higher NaOH concentrations. This observation is likely attributable to the balance between ion-exchange (favoring desorption) and electrostatic repulsion (inhibiting desorption).

In order to conduct an assessment of reusability and stability for the adsorption of MP, the adsorption–desorption cycle was repeated three times using the same adsorption materials as shown in Table 5. Reusability was an important factor in evaluating the performance of adsorption on GO/Fe_3O_4. The results revealed that GO/Fe_3O_4 was recyclable by magnetic force and remained stable during the third cycles. The loss (less than 20%) of adsorption capacity for GO/Fe_3O_4 may be ascribed to the detachment of the shell (graphene) during the third cycle. Further studies are necessary to develop strategies, which will prohibit the separation of the shell from the core and retain the performance of the prepared magnetic adsorbent.

4. Conclusions

The magnetic nanoadsorbents (GO/Fe_3O_4) were successfully synthesized for the adsorption of Ni(II), MP, and RB5 and can be easily recovered from treated water by magnetic force without further downstream treatment. Under the studies' conditions, the maximum adsorption capacity of GO/Fe_3O_4 followed the order of RB5 (63.18 mg g^{-1}) > MP (20.69 mg g^{-1}) > Ni(II) (15.5 mg g^{-1}), possibly due to π–π interactions and electrostatic attraction. The adsorption efficiencies of RB5 in alkaline solutions (pH 8 to pH 10) were also lower than that in acidic solutions (from pH 2 to 6), due to the electrostatic repulsion between the anionic dye RB5 and the negatively charged GO/Fe_3O_4 surface in alkaline solutions. The results for the removal of Ni(II), MP, and RB5 onto GO/Fe_3O_4 revealed that equilibrium data were well fitted by the Langmuir model, and kinetic data followed a pseudo-second-order model, which suggests that the adsorption process is quite rapid and is probably dominated by a chemical adsorption phenomenon. The optimum conditions for desorption of Ni(II), MP, and RB5 was 0.1 M HNO_3, 95% ethanol, and 0.1 NaOH, respectively. As expected, GO/Fe_3O_4 will open up the potential for broad applications owing to the higher reusability, magnetic recovery, and adsorption capacity of Ni(II), MP, and RB5 in the wastewater treatment.

Acknowledgments

This research was supported in part by Grant MOST 109-2622-E-197-002 -CC3 from the Ministry of Science and Technology, Republic of China.

References

[1] B.K. Zaied, M. Rashid, M. Nasrullah, A.W. Zularisam, D. Pant, L. Singh, A comprehensive review on contaminants removal from pharmaceutical wastewater by electrocoagulation process, Sci. Total Environ., 726 (2020) 138095. 10.1016/j.scitotenv.2020.138095.
[2] J. Li, Y. Zheng, X. Feng, C. Lv, X. Liu, Y. Zhao, L. Chen, Adsorption removal of Ni(II) and phenol from aqueous solution by modified attapulgite and its composite hydrogel, Environ. Technol, (2019) 1–15. 10.1080/09593330.2019.1703821.
[3] M.R. Samarghandi, J.K. Yang, S.M. Lee, O. Giahi, M. Shirzad-Siboni, Effect of different type of organic compounds on the photocatalytic reduction of Cr(VI) in presence of ZnO nanoparticles, Desal. Water Treat., 52 (2014) 1531–1538.
[4] Y. Wu, B. Li, X. Wang, S. Yu, H. Pang, Y. Liu, X. Liu, X. Wang, Magnetic metal-organic frameworks (Fe_3O_4@ZIF-8) composites

for U(VI) and Eu(III) elimination: simultaneously achieve favorable stability and functionality, Chem. Eng. J., 378 (2019) 122105. 10.1016/j.cej.2019.122105.
[5] M. Samadi, M. Saghi, A. Rahmani, J. Hasanvand, S. Rahimi, M.S. Syboney, Hamadan landfill leachate treatment by coagulation-flocculation process, J. Environ. Health Sci. Eng., 7 (2010) 253–258.
[6] R.D.R. Silva, R.T. Rodrigues, A.C. Azevedo, J. Rubio, Calcium and magnesium ion removal from water feeding a steam generator by chemical precipitation and flotation with micro and nanobubbles, Environ. Technol., 41 (2020) 1–20. 10.1080/09593330.2018.1558288.
[7] M. Mokhter, S. Lakard, C. Magnenet, M. Euvrard, B. Lakard, Preparation of polyelectrolyte-modified membranes for heavy metal ions removal, Environ. Technol., 38 (2017) 2476–2485.
[8] S. Gámez, K. Garcés, E. Torre, A. Guevara, Precious metals recovery from waste printed circuit boards using thiosulfate leaching and ion exchange resin, Hydrometallurgy, 186 (2019) 1–11.
[9] M. Matsumiya, Y. Song, Y. Tsuchida, Y. Sasaki, Separation of palladium by solvent extraction with methylamino-bis-N,N-dioctylacetamide and direct electrodeposition from loaded organic phase, Sep. Purif. Technol., 234 (2020) 115841. 10.1016/j.seppur.2019.115841.
[10] X. Wang, X. Liu, C. Xiao, H. Zhao, M. Zhang, N. Zheng, W. Kong, L. Zhang, H. Yuan, L. Zhang, J. Lu, Triethylenetetramine-modified hollow Fe_3O_4/SiO_2/chitosan magnetic nanocomposites for removal of Cr(VI) ions with high adsorption capacity and rapid rate, Microporous Mesoporous Mater., 297 (2020) 110041. 10.1016/j.micromeso.2020.110041.
[11] M. Shirzad-Siboni, S.-J. Jafari, M. Farrokhi, J.K. Yang, Removal of phenol from aqueous solutions by activated red mud: equilibrium and kinetics studies, Environ. Eng. Res., 18 (2013) 247–252.
[12] M. Shirzad-Siboni, A. Khataee, F. Vafaei, S.W. Joo, Comparative removal of two textile dyes from aqueous solution by adsorption onto marine-source waste shell: kinetic and isotherm studies, Korean J. Chem. Eng., 31 (2014) 1451–1459.
[13] S. Salahi, M. Ghorbani, Adsorption parameters studies for the removal of mercury from aqueous solutions using hybrid sorbent, Adv. Polym. Technol., 33 (2014) 21428. 10.1002/adv.21428.
[14] X. Hu, J. Kang, K. Lu, R. Zhou, L. Mu, Q. Zhou, Graphene oxide amplifies the phytotoxicity of arsenic in wheat, Sci. Rep., 4 (2014) 1–10.
[15] W.S. Hummers, R.E. Offeman, Preparation of graphitic oxide, J. Am. Chem. Soc., 80 (1958) 1339.10.1021/ja01539a017.
[16] S. Khan, A.A. Edathil, F. Banat, Sustainable synthesis of graphene-based adsorbent using date syrup, Sci. Rep., 9 (2019) 18106.
[17] M.M. Galangash, M.M. Montazeri, A. Ghavidast, M. Shirzad-Siboni, Synthesis of carboxyl-functionalized magnetic nanoparticles for adsorption of malachite green from water: kinetics and thermodynamics studies, J. Chin. Chem. Soc., 65 (2018) 940–950.
[18] A. Mohagheghian, R. Vahidi-Kolur, M. Pourmohseni, J.K. Yang, M. Shirzad-Siboni, Application of scallop shell-Fe_3O_4 nanocomposite for the removal Azo dye from aqueous solutions, Water Air Soil Pollut., 226 (2015) 321.
[19] A. Mohagheghian, M. Pourmohseni, R. Vahidi-Kolur, J. Yang, M. Shirzad-Siboni, Application of kaolin-Fe_3O_4 nano-composite for the removal azo dye from aqueous solutions, Desal. Water Treat., 58 (2017) 308–319.
[20] H.W. Chen, C.S. Chiou, S.H. Chang, Comparison of methylparaben, ethylparaben and propylparaben adsorption onto magnetic nanoparticles with phenyl group, Powder Technol., 311 (2017) 426–431.
[21] F. Andersen, Final amended report on the safety assessment of methylparaben, ethylparaben, propylparaben, isopropylparaben, butylparaben, isobutylparaben, and benzylparaben as used in cosmetic products, Int. J. Toxicol., 27 (2008) 1–82.
[22] M.Y. Shin, C. Shin, J.W. Choi, J. Lee, S. Lee, S. Kim, Pharmacokinetic profile of propyl paraben in humans after oral administration, Environ. Int., 130 (2019) 104917. 10.1016/j.envint.2019.104917.
[23] D. Błędzka, J. Gromadzińska, W. Wąsowicz, Parabens. From environmental studies to human health, Environ. Int., 67 (2014) 27–42.
[24] M. Pedrouzo, F. Borrull, R.M. Marcé, E. Pocurull, Ultra-high-performance liquid chromatography–tandem mass spectrometry for determining the presence of eleven personal care products in surface and wastewaters, J. Chromatogr. A, 1216 (2009) 6994–7000.
[25] V. Coman, B. Robotin, P. Ilea, Nickel recovery/removal from industrial wastes: a review, Resour. Conserv. Recycl., 73 (2013) 229–238.
[26] E. Salihi, J. Wang, D. Coleman, L. Šiller, Enhanced removal of nickel(II) Ions from aqueous solutions by SDS-functionalized graphene oxide, Sep. Sci. Technol., 51 (2016) 1317–1327.
[27] A.C.d. Groot, E.G. Beverdam, C.T. Ayong, P.J. Coenraads, J.P. Nater, The role of contact allergy in the spectrum of adverse effects caused by cosmetics and toiletries, Contact Dermatitis, 19 (1988) 195–201.
[28] H.A. Begum, A.K. Mondal, T. Muslim, Adsorptive removal of Reactive Black 5 from aqueous solution using chitin prepared from shrimp shells, Bangladesh Pharm. J., 15 (2012) 145–152.
[29] F.J. Ruiz-Duenas, M. Morales, M.J. Mate, A. Romero, M.J. Martinez, A.T. Smith, A.T. Martinez, Site-directed mutagenesis of the catalytic tryptophan environment in *Pleurotus eryngii* versatile peroxidase, Biochemistry, 47 (2008) 1685–1695.
[30] F. Yue, Q. Zhang, L. Xu, Y. Zheng, C. Yao, J. Jia, W. Leng, S. Hou, Porous reduced graphene oxide/single-walled carbon nanotube film as freestanding and flexible electrode materials for electrosorption of organic dye, ACS Appl. Nano Mater., 2 (2019) 6258–6267.
[31] C.S. Chiou, K.J. Chuang, H.W. Chen, Y.C. Chen, Magnetite modified with amine polymer to adsorb indium ions, Powder Technol., 279 (2015) 247–253.
[32] Y. Yan, S. Sun, Y. Song, X. Yan, W. Guan, X. Liu, W. Shi, Microwave-assisted in situ synthesis of reduced graphene oxide-$BiVO_4$ composite photocatalysts and their enhanced photocatalytic performance for the degradation of ciprofloxacin, J. Hazard. Mater., 250–251 (2013) 106–114.
[33] L.H. Jiang, Y.G. Liu, G.M. Zeng, F.Y. Xiao, X.J. Hu, X. Hu, H. Wang, T.T. Li, L. Zhou, X.F. Tan, Removal of 17β-estradiol by few-layered graphene oxide nanosheets from aqueous solutions: external influence and adsorption mechanism, Chem. Eng. J., 284 (2016) 93–102.
[34] D. Schaumlöffel, Nickel species: analysis and toxic effects, J. Trace Elem. Med. Biol., 26 (2012) 1–6.
[35] J. Xiao, W. Lv, Z. Xie, Y. Tan, Y. Song, Q. Zheng, Environmentally friendly reduced graphene oxide as a broad-spectrum adsorbent for anionic and cationic dyes via π–π interactions, J. Mater. Chem. A, 4 (2016) 12126–12135.
[36] M.M. Felista, W.C. Wanyonyi, G. Ongera, Adsorption of anionic dye (Reactive black 5) using macadamia seed Husks: kinetics and equilibrium studies, Sci. Afr., 7 (2020) e00283.10.1016/j.sciaf.2020.e00283.
[37] S. Zhao, J. Zang, M. Zhu, Y. Zhang, Z. Liu, Y. Ma, Y. Zhu, C. Zhang, Effects of functional groups on the structure, physicochemical and biological properties of mesoporous bioactive glass scaffolds, J. Mater. Chem. B, 3 (2015) 1612–1623.
[38] M. Zhang, Q. Yin, X. Ji, F. Wang, X. Gao, M. Zhao, High and fast adsorption of Cd(II) and Pb(II) ions from aqueous solutions by a waste biomass based hydrogel, Microporous Mesoporous Mater., 10 (2020) 1–13.10.1038/s41598–020-60160-w.
[39] P. Lin, J. Wu, J. Ahn, J. Lee, Adsorption characteristics of Cd(II) and Ni(II) from aqueous solution using succinylated hay, Int. J. Miner. Metall. Mater., 26 (2019) 1239–1246.

[40] P. Lin, J. Wu, J. Ahn, J. Lee, Thermodynamics, kinetics, and activation energy studies of the sorption of chromium(III) and chromium(VI) to a Mn_3O_4 nanomaterial, Chem. Eng. J., 254 (2014) 374–383.
[41] F. Chen, C. Zhou, G. Li, F. Peng, Thermodynamics and kinetics of glyphosate adsorption on resin D301, Arab. J. Chem., 9 (2016) S1665-S1669.
[42] J.H. Deng, X.R. Zhang, G.M. Zeng, J.L. Gong, Q.Y. Niu, J. Liang, Simultaneous removal of Cd(II) and ionic dyes from aqueous solution using magnetic graphene oxide nanocomposite as an adsorbent, Chem. Eng. J., 226 (2013) 189–200.
[43] S. Bekkouche, S. Baup, M. Bouhelassa, S. Molina-Boisseau, C. Petrier, Competitive adsorption of phenol and heavy metal ions onto titanium dioxide (Dugussa P25), Desal. Water Treat., 37 (2012) 364–372.